Stability diagram of unilateral buckling patterns of strip-delaminated films

G. Parry, A. Cimetière, C. Coupeau,* J. Colin, and J. Grilhé
Laboratoire de Métallurgie Physique, UMR 6630 du CNRS, Université de Poitiers, BP 30179, 86962 Futuroscope Cedex, France
(Received 25 July 2006; published 5 December 2006)

Thin films deposited on substrates are usually submitted to large residual compression stresses, causing delamination and buckling of the film into various patterns. The present study is focused on the different equilibria arising on strip-shaped delaminated areas. The three most common types of buckling patterns observed on such strips are known as the straight-sided wrinkles, bubble pattern, and telephone cord blisters. The stability of those equilibria as a function of the two stress components of the loading is investigated. The Föppl–Von Karman model for elastic plates is used for theoretical aspects. The post-critical equilibrium paths of the buckling patterns are investigated numerically by means of the finite-element method. The substrate is assumed to be rigid and the contact to be frictionless. The equilibrium solutions can be classified into families of homologous equilibria allowing the identification of dimensionless parameters for the study of stability. A mapping of the different stable post-critical equilibria is given. It is shown that the straight-sided wrinkles and the bubbles are associated with anisotropy of stresses and/or of elastic properties, whereas the telephone cords are stable at high isotropic stresses. The morphological transitions are experimentally evidenced by *in situ* atomic force microscopy observations of a nickel 50-nm-thick film under stress.

DOI: 10.1103/PhysRevE.74.066601 PACS number(s): 46.25.Cc, 46.32.+x, 68.60.Bs, 68.37.Ps

I. INTRODUCTION

The buckling and delamination of stressed multilayers have been widely investigated in the frame of solid mechanics [1–7] and materials science [8]. Coatings are involved in a wide range of technological applications, including microelectronic or corrosion barriers. Buckling phenomena are also arising in other fields. In biology, for instance, plate buckling is studied to understand the patterns associated with some vegetable organism formation [9]. In the field of material sciences and metallurgy, the metallic thin films deposited on substrates by sputtering methods may lead to very high compressive stresses that are susceptible to inducing delamination and buckling resulting in various structures, such as straight-sided blisters, telephone cord, or bubble patterns [10–14]. Similar patterns can be observed in larger-scale structures with mode jumping in thermally buckled plates [15] or can be induced by post-irradiation [16].

Such buckling patterns, as well as most of the examples cited above, have been investigated in the frame of the Von Karman theory of plates. It is now well known that the telephone cords and bubble patterns are two buckling modes of the straight-sided wrinkle and hence are known as secondary buckling. Some quantities, such as optimal wavelengths and critical values of the biaxial stress loading, associated with those secondary buckling structures, have been already discussed, but only in the framework of linear stability analysis of the straight-sided blister [12,17,18]. More recently, a post-buckling analysis, associated with a frictionless contact problem between the film and the substrate, has given way to a better understanding of the buckling transitions. The variation of the optimal wavelength of the bubble patterns during biaxial stress-state evolution has been highlighted [19], and a snap-through phenomenon has been shown to occur under specific conditions during the straight-sided wrinkle to bubble transition [20]. The ratio between longitudinal and transversal stress components appears as the critical parameter for the bifurcations.

The aim of this study is to obtain a stability diagram for the thin-film post-buckling equilibria. In order to exhibit relevant dimensionless characteristic parameters, equilibrium solutions are gathered into homologous equilibrium families. Any solution for a single family allows building all the other equilibria of the family. Hence, a few numerical calculations are needed to determine the stability diagram. The formation of straight-sided blisters on metallic films and their evolution toward bubbles and telephone cord blisters are experimentally investigated with the help of an original device [21,22]. The samples, composed of metallic thin films deposited on polycarbonate substrates, are uniaxially compressed while the film surface is observed *in situ* by atomic force microscopy (AFM). The different stages of the transitions are observed as the biaxial stress state is modified by the external compression. The numerical results are finally compared to these experimental data.

II. MODELING OF THE BUCKLING PROBLEM

The present study is focused on the buckling arising on straight-sided delaminated strips. These structures cannot be only analyzed within the framework of incipient buckling of the straight-sided blisters, since the loading levels induce advanced post-critical buckling, far from the initial bifurcation point [19].

The delaminated areas are regarded as rectangular strips of infinite length and width b resulting from the delamination. The strip width is oriented along the Oy direction and the length is aligned with the Ox direction. It is assumed that the width b remains constant during the buckling, with no crack propagation at the film/substrate interface. The film is

*Electronic address: christophe.coupeau@univ-poitiers.fr

modeled as an elastic plate of thickness h, Yong's modulus E, and Poisson's ratio ν.

A frictionless contact model between the film and the substrate is chosen. This is hence a unilateral buckling problem, since the film cannot penetrate into in the half space occupied by the substrate. Numerical computations show that the contact areas may actually become relatively wide as the equilibria go further in the post-critical regime.

Geometrically nonlinear plate models have to be considered in this problem in order to study the buckling modes, but also in order to follow the post-critical equilibrium paths and to deal with the transitions between the different patterns. The Föppl–Von Karman model is used to discuss theoretical results. For the numerical calculations, the geometrical nonlinear Green-Lagrange strain tensor is computed.

The elastic plate is clamped along the edges. The substrate is assumed to impose displacements at the boundaries of the delaminated area. Those displacements can be readily related to the stresses measured in the adherent part of the film. The film is clamped to the substrate along the two sides of the strip.

III. FAMILIES OF HOMOLOGOUS EQUILIBRIA

The aim of this section is to show how knowledge of a particular equilibrium in one of the above-depicted types allows one to build an infinity of equilibria of the same type. The whole set of those so-build equilibria is here called the set of homologous equilibria, for reasons that will be developed further. This family building strategy is convenient for finding the relevant parameters for the study of stability.

Let us denote by (u,v,w) the components of the film displacement along the axis (Ox,Oy,Oz), respectively. The components u and v are in-plane displacements, while w is the out-of-plane displacement. The different plates considered are made of the same homogeneous elastic material of Young's modulus E and Poison's ratio ν. Their thickness h and width b may be different. No particular assumption has to be taken for the shape of the delaminated zone (i.e., of the plate) in the following discussion of the current section.

Let us consider a particular reference configuration $\mathcal{E}^0$ for a film relying on the rigid substrate. Let us denote by (u^0,v^0,w^0) the three displacement components, h^0 the film thickness, and N^0 the in-plane stress integrated in the plate thickness. Finally, let $\alpha>0$ be a constant. A new field (u,v,w) can be defined from the displacement field (u^0,v^0,w^0) by

$$u(X,Y)=\frac{1}{\alpha}\left(\frac{h}{h^0}\right)^2 u^0\left(\frac{X}{\alpha},\frac{Y}{\alpha}\right),$$

$$v(X,Y)=\frac{1}{\alpha}\left(\frac{h}{h^0}\right)^2 v^0\left(\frac{X}{\alpha},\frac{Y}{\alpha}\right),$$

$$w(X,Y)=\left(\frac{h}{h^0}\right) w^0\left(\frac{X}{\alpha},\frac{Y}{\alpha}\right), \tag{1}$$

with $X=\alpha x$ and $Y=\alpha y$.

The constant α is a similarity ratio in the (Ox,Oy) plane. The new plate in the (Ox,Oy) plane is similar to the reference plate. Nevertheless, the two displacement fields are not similar, since the factor that multiplies the in-plane components u and v is not the same as the factor for w. The (u,v,w) field will be shown further to be a solution of the Von Karman equations, hence to describe an equilibrium $\mathcal{E}$ of the same kind as the original one.

The Von Karman strain tensor e for the new displacement field can be formulated as a function of the strain tensor e^0 in the reference state

$$e_{XX}=\frac{\partial u}{\partial X}+\frac{1}{2}\left(\frac{\partial w}{\partial X}\right)^2=\frac{1}{\alpha^2}\left(\frac{h}{h^0}\right)^2\left[\frac{\partial u^0}{\partial x}+\frac{1}{2}\left(\frac{\partial w^0}{\partial x}\right)^2\right]$$
$$=\frac{1}{\alpha^2}\left(\frac{h}{h^0}\right)^2 e^0_{xx},$$

$$e_{YY}=\frac{\partial v}{\partial Y}+\frac{1}{2}\left(\frac{\partial w}{\partial Y}\right)^2=\frac{1}{\alpha^2}\left(\frac{h}{h^0}\right)^2 e^0_{yy},$$

$$e_{XY}=\frac{1}{2}\left(\frac{\partial u}{\partial Y}+\frac{\partial v}{\partial X}\right)+\frac{1}{2}\frac{\partial w}{\partial X}\frac{\partial w}{\partial Y}=\frac{1}{\alpha^2}\left(\frac{h}{h^0}\right)^2 e^0_{xy}. \tag{2}$$

The new stress tensor N can be formulated as a function of the reference-state stress tensor N^0:

$$N_{XX}=\frac{Eh}{(1-\nu^2)}\frac{1}{\alpha^2}\left(\frac{h}{h^0}\right)^2[e^0_{xx}+\nu e^0_{yy}]=\frac{1}{\alpha^2}\left(\frac{h}{h^0}\right)^3 N^0_{xx},$$

$$N_{YY}=\frac{Eh}{(1-\nu^2)}\frac{1}{\alpha^2}\left(\frac{h}{h^0}\right)^2[e^0_{yy}+\nu e^0_{xx}]=\frac{1}{\alpha^2}\left(\frac{h}{h^0}\right)^3 N^0_{yy},$$

$$N_{XY}=\frac{Eh}{(1+\nu)}\frac{1}{\alpha^2}\left(\frac{h}{h^0}\right)^2[e^0_{xy}]=\frac{1}{\alpha^2}\left(\frac{h}{h^0}\right)^3 N^0_{xy}. \tag{3}$$

The e and N tensors are proportional to e^0 and N^0, respectively. Let Δ^2 be the bilaplacian and $\nabla\nabla$ the bigradient, both with respect to X and Y. It is straightforward to verify that the Von Karman equations are satisfied for (u,v,w)

$$\frac{Eh^3}{12(1-\nu^2)}\Delta^2 w-N:\nabla\nabla w=0. \tag{4}$$

By mean of this transformation, a whole family of equilibria can be found by varying the two parameters h/h_0 and α without any further calculation. For a given film of thickness h, the stress is given by

$$N=\left(\frac{1}{\alpha}\right)^2\left(\frac{h}{h^0}\right)^3 N^0. \tag{5}$$

The new displacement field can be calculated from (1).

In the following developments, the equilibrium states appearing on strips (i.e., the straight-sided wrinkles, the bubble, and the telephone cord patterns) will be dealt with. In this case, a rectangular strip of width b_0 is transformed into a rectangular strip of width b and the in-plane similarity factor is $\alpha=\frac{b}{b_0}$. Relation (5) can be then written in the form $Nb^2/h^3=N^0(b^0)^2/(h^0)^3$. The quantity Nb^2/h^3 is invariant

within a family. Within a family of homologous equilibria the out-of-plane displacement and the tension in the middle plane are related by

$$w(X,Y)/h = w^0\left(\frac{b_0}{b}X, \frac{b_0}{b}Y\right) \Big/ h^0,$$

$$\sigma = \left(\frac{h}{h_0}\right)^2\left(\frac{b_0}{b}\right)^2\sigma^0. \tag{6}$$

In the case of the bubbles and telephone cord equilibria, the post-critical regimes can not be analytically obtained and numerical computations are required. However, the above result allows one to reduce significantly the required number of computations. For instance, let us consider a strip of width b and thickness h, submitted to the biaxial loading σ. In order to know the various equilibrium states, one only needs to know the equilibrium states on a strip of width b_0 and thickness h_0 submitted to a biaxial stress:

$$\sigma^0 = \left(\frac{h_0}{h}\right)^2\left(\frac{b}{b_0}\right)^2\sigma. \tag{7}$$

This means that the numerical calculations only need to be carried out on one film of width b_0 and thickness h_0.

IV. STABILITY DIAGRAM FOR THE BUCKLING PATTERNS

The loading on the elastic strip is deduced from the biaxial stress state in the adherent part of the film. This biaxial stress state can be conveniently decomposed in two components σ_l and σ_t. These quantities σ_l and σ_t are the compression applied to the elastic strip, respectively longitudinally [(Ox) direction] and transversally [(Oy) direction] with respect to the strip.

Previous studies have highlighted the influence of the ratio σ_l/σ_t on the stability of the various patterns. A first stability diagram in the (σ_t, σ_l) plane is given in [18]. It is based on the perturbation of the straight-sided wrinkle solution, analytically known by introducing some shape functions imitating the secondary buckling equilibria. Though this method gives interesting results, the unilateral nature of the problem, especially the formation of contact areas between the film and the substrate, is not taken into account. These contact areas, however, become quite large in the post-critical regime for equilibria far from the straight-sided wrinkle equilibrium in terms of loading.

In the adherent plane part of the film, the stress components are uniform in thickness, resulting in the equalities $\sigma_t = N_t/h$ and $\sigma_l = N_l/h$. Inside a given family of homologous equilibria, the loading can be defined by the invariant couple $(\sigma_t b^2/h^2, \sigma_l b^2/h^2)$. The stability diagram, which is a kind of phase diagram of all the known equilibria potentially developing on a strip, is given in the two-dimensional space (β_t, β_l), with

$$\beta_t = \frac{\sigma_t}{\bar{E}}\left(\frac{b}{h}\right)^2, \quad \beta_l = \frac{\sigma_l}{\bar{E}}\left(\frac{b}{h}\right)^2, \tag{8}$$

where $\bar{E} = \frac{E}{1-\nu^2}$.

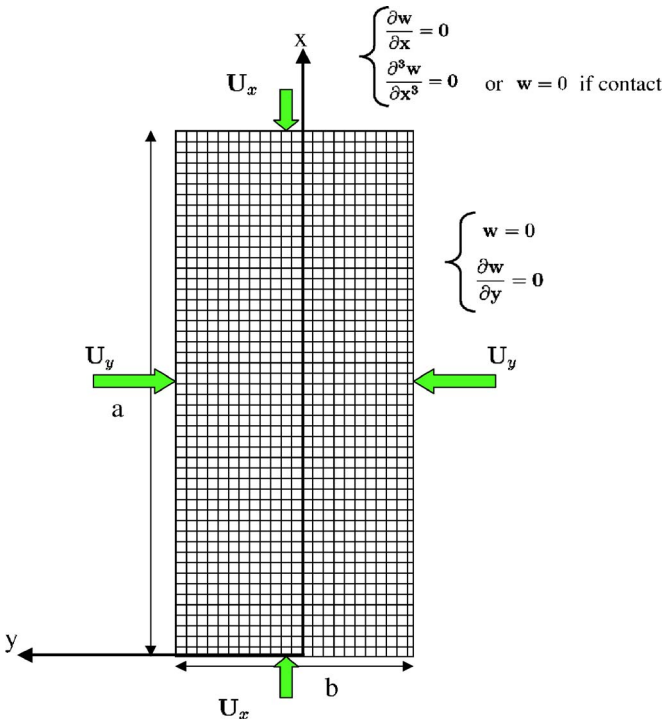

FIG. 1. (Color online) Film strip section of width b and length a. The FEM mesh is constituted of quadrilateral shell elements. The film is clamped to the substrate along the delaminated edge $(y=-b/2, y=+b/2)$ and symmetry conditions are applied to the transversal edges $(x=0, x=a)$.

As explained previously, the whole (β_t, β_l) space is investigated from calculations carried out on a strip of given geometrical characteristics by varying the parameters (β_t, β_l) through the loading (σ_t, σ_l). Each point of the diagram is associated with a family of homologous equilibria. The whole diagram represents all the equilibria in all the families independently of the geometry.

Numerical calculations have been carried out using the ABAQUS finite-element (FEM) software [23] in order to determine the post-buckling regime. It is noted that the bubbles and telephone cord patterns are assumed to be constituted of unit cells repeated periodically along the strip. Let us denote by a this unit-cell length. The finite-element model can then be reduced to a rectangular plate of length a, width b, and thickness h (Fig. 1). The plate is meshed with quadrilateral shell elements. The influence of the spatial periodicity can be investigated by varying a. Two kinds of boundary conditions are applied along the edges of the plate and are depicted in Fig. 1: along the delamination front [(Ox) direction], the plate is clamped to the substrate $\left(w=0, \frac{\partial w}{\partial y}=0\right)$; for the edges lying along the width of the strip [(Oy) direction], boundary conditions taking into account the periodicity are prescribed (Fig. 1).

The substrate is taken into account by the introduction of a rigid plane preventing the film from going into the $(z<0)$ half-space. The geometrical nonlinear Green-Lagrange strain tensor is computed during the resolution in order to account for large displacements. The loading consists in displacements U_x and U_y prescribed along the edges of the plate

and computed from the biaxial stress components σ_t and σ_l in the adherent part of the film.

The aim of the mapping is the determination of the most stable equilibrium pattern for each value of (β_t, β_l). A numerical exploration has to be carried out in (β_t, β_l) space in order to identify the boundaries of four areas, each one corresponding to a given kind of buckling pattern. These areas will be referenced as stability areas. Each loading can be represented by a line drawn from the origin point (0, 0) to a destination point (β_t^f, β_l^f). The destination (β_t^f, β_l^f) must be chosen such that the loading path crosses one of the different stability area boundaries. The loading path leading from (0, 0) to (β_t^f, β_l^f) can be decomposed into several segments arbitrarily chosen. For instance, it is sometimes convenient that the loading first reach an intermediate point $(0, \beta_l^f)$ or $(\beta_t^f, 0)$ before reaching the final destination.

For a given loading, let m be the number of potential equilibria, $1 \leqslant m \leqslant 4$. For each given equilibrium—i.e., for a given $k \in \{1, \ldots, m\}$, a strain energy $E^k(\beta_t, \beta_l, a)$ can be computed. The quantity which is relevant for comparison between equilibria is the strain energy per unit length $e^k(a) = E^k/a$. In the case of a straight-sided blister, which is geometrically invariant with respect to translation in the Ox direction, a can be arbitrarily chosen. For a given kind of periodic structure (bubbles or telephone cords), the spatial period $l^k(\beta_t, \beta_l)$ corresponding to the most stable structure is selected as the value of a minimizing the energy density e^k. The corresponding value of e^k is denoted e^{*k}. The equilibrium k for which e^{*k} is minimum is then selected. The loading is increased linearly and proportionally to a dimensionless parameter τ. The parameter τ will be used to follow the loading progression. It is thus possible to follow the evolution of $e^{*i}(\tau)$, $i \in \{1, \ldots, m\}$, as the loading is progressively applied. A boundary is crossed when, for $i \neq j$, $e^{*i}(\tau) = e^{*j}(\tau)$.

This method for the determination of the stability area boundaries is illustrated in Fig. 2 with two examples of loadings ($\mathcal{L}_1$ and $\mathcal{L}_2$). The variations of $e^{*k}(\tau)$ are followed in order to identify the values of τ for which one of the boundaries is getting crossed [Fig. 2(a)]. At the first stages of the $\mathcal{L}_1$ loading ($\tau \leqslant \tau_{c1}$), the plane state is the only equilibrium solution. Over a critical value τ_{c1} of τ, a bifurcation occurs, leading to a bubble equilibrium. The point $(\beta_t(\tau_{c1}), \beta_l(\tau_{c1}))$ thus marks the limit between the bubbles and the plane stability areas [Fig. 2(b)]. A telephone cord equilibrium can arise for τ slightly over τ_{c1}. The telephone cord structure is nevertheless less stable than the bubble structure $[e^{*\text{bubble}}(\tau) < e^{*\text{cord}}(\tau)]$ until τ reaches the value τ_{c2}. Over this value, the telephone cord equilibrium remains the most stable pattern. This procedure is carried out for several loadings.

The buckling shapes obtained by FEM calculations are reported in Fig. 2(c). Note that the amplitude is multiplied by a factor of about 10 in order to clearly identify the various buckling structures. The initial plane state is identified by (P). For the $\mathcal{L}_1$ path, the incipient buckling of the plan film into the bubble mode (B) occurs just upon τ_{c1}. For increasing values of τ, the bubble is getting going into its postcritical-regime (B). The telephone cord buckle (T) is stable for τ higher than τ_{c2}. The $\mathcal{L}_2$ path is characterized by a first transition to straight-sided wrinkle (S) and a second one to the telephone cord structure (T).

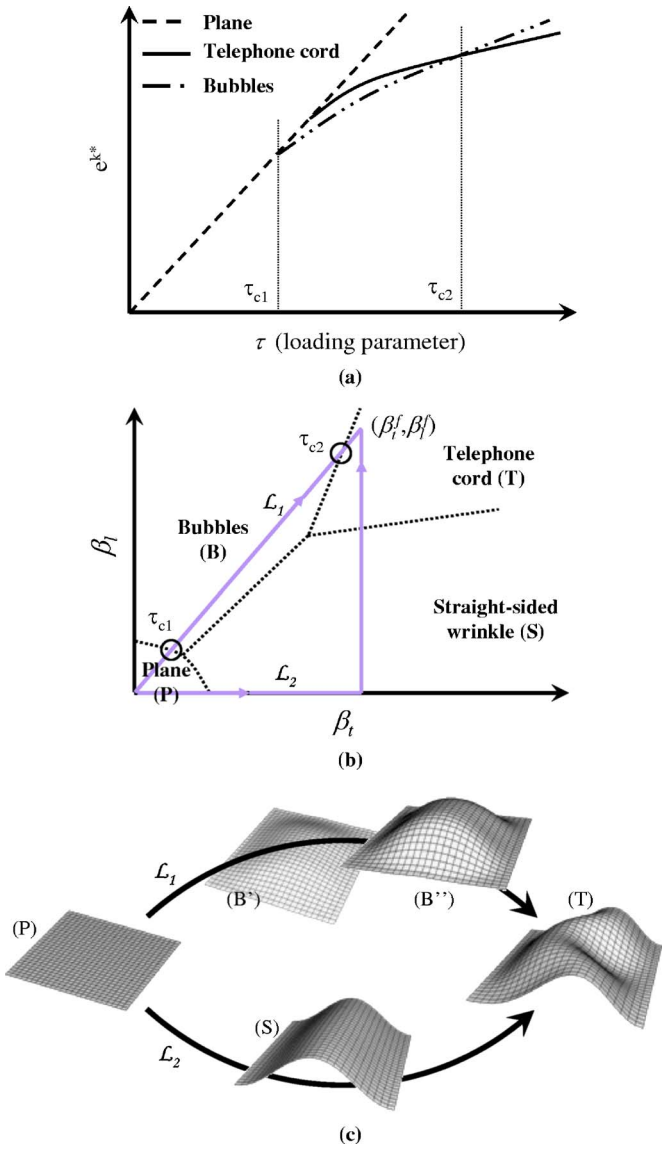

FIG. 2. (Color online) Method for determining the stability areas of the buckling structure. (a) Energy for the different equilibria (plane, telephone cords, and bubbles) along the loading path $\mathcal{L}_1$. For each loading state, the equilibrium of minimum energy is selected as the stable one. Area boundaries are identified by curve crossings, at τ_{c1} and τ_{c2}, for instance. (b) Calculations carried out in the (β_t, β_l) space for the two different loading paths $\mathcal{L}_1$ and $\mathcal{L}_2$. The critical loading parameters τ_{c1} and τ_{c2} evidenced in (a) for the path $\mathcal{L}_1$ have been reported. They characterize the stability domains boundaries. (c) FEM buckling shape associated with the two loading paths $\mathcal{L}_1$ and $\mathcal{L}_2$. (P), (B), (T), and (S) correspond to the plane state, the bubbles, the telephone cord, and the straight-sided wrinkle, respectively.

The stability diagram established by this method is represented Fig. 3. Four different areas are visible in the diagram, each of them associated with a given equilibrium pattern. For the small values of both loading parameters β_t and β_l, the plane state is the only equilibrium solution. The correspond-

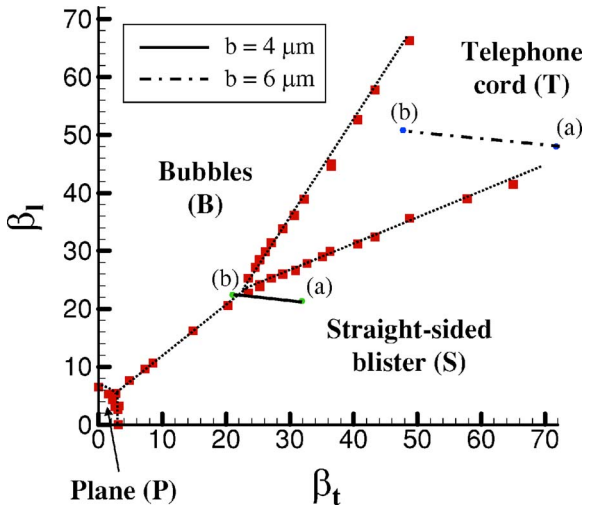

FIG. 3. (Color online) FEM stability diagram of the buckling structures. The two nondimensional parameters used for the mapping are $\beta_t = \sigma_t \frac{1-\nu^2}{E}\left(\frac{b}{h}\right)^2$ and $\beta_l = \sigma_l \frac{1-\nu^2}{E}\left(\frac{b}{h}\right)^2$, where σ_t and σ_l are the transversal and longitudinal stresses, respectively, E and ν are the film Young's modulus and Poisson's coefficient, respectively, h is the film thickness, and b is the strip width. Four stability domains are evidenced: the plane state, the bubbles, the straight-sided wrinkle, and the telephone cord structure. Experimental loadings labelled (a) and (b) presented in Fig. 4 have been reported in the diagram, for both 4 and 6 μm strip widths experimentally studied.

ing area is centred on the origin (0, 0). Beyond this area the bubble and straight-sided patterns seem to be on both sides of a bisector. As expected for given strip width and film thickness, an excess in the lateral compression (β_t) promotes the formation of straight-sided blisters, whereas an excess in the longitudinal compression (β_l) is favorable for the bubble pattern. The telephone cord pattern is stable for higher stress levels. The experimental observations of bubbles and straight-sided wrinkles are consequently evidence of a strong anisotropy of stress (σ_l/σ_t ratio) or of the elastic properties (E, ν) in the considered thin films. Moreover, it is interesting to note that the state of high equibiaxial stresses is located in the telephone cord area. This may explain why this structure spontaneously develops in most of the highly stressed thin films and coatings elaborated by sputtering methods.

The diagram is consistent with the well-known results of the straight-sided wrinkle formation. The analytical value of the critical stress for which a plane plate of infinite length and width b submitted to a lateral compressive loading σ_t buckles into a straight-sided wrinkle is

$$\sigma_t = 4\frac{\pi^2 D}{hb^2}, \tag{9}$$

where $D = \frac{Eh^3}{12(1-\nu^2)}$ is the plate flexion modulus.

The longitudinal stress component σ_l has no influence on this transition, since the straight-sided solution is invariant along the longitudinal direction. The corresponding critical value for β_t is $\beta_t^c = \frac{\pi^2}{3}$ [1], in good agreement with the boundary between the plane and straight-sided domains in Fig. 3. The upper end point of this segment is located on the boundary of the bubble area. This is a "triple point" where all the three equilibria—plane state, bubbles, and straight-sided wrinkles—coexist. The stability diagram exhibits also another triple point at the boundary of the bubbles, the straight-sided wrinkles, and the telephone cord blisters, located at $(\beta_t, \beta_l) = (21, 21)$.

V. EXPERIMENTAL RESULTS

The mechanical behavior of thin films has been investigated using an experimental apparatus allowing *in situ* AFM observations of sample surfaces during deformation [21]. The details of the experimental protocol can be found in [19]. Nickel 50-nm-thick films have been deposited on polycarbonate substrates at room temperature using an ion beam sputtering. The as-deposited thin films present initial residual compressive and equibiaxial stresses σ_0, estimated by curvature and $\sin^2\psi$ x-ray diffraction (XRD) methods. In order to induce delamination and buckling of the initially well-adherent film, the substrate is first compressed along the (Oy) axis. During the uniaxial compression, external stresses $(\Delta\sigma_{xx}, \Delta\sigma_{yy})$ are generated in the film:

$$\Delta\sigma_{xx} = \frac{E_f}{E_s}\frac{\nu_f - \nu_s}{1-\nu_f^2}\sigma_{ext},$$

$$\Delta\sigma_{yy} = \frac{E_f}{E_s}\frac{1-\nu_s\nu_f}{1-\nu_f^2}\sigma_{ext},$$

where E_i and ν_i are Young's modulus and Poisson's ratio of the material (i), respectively, and σ_{ext} is the external stress applied to the polycarbonate substrate during the experiment. The total stress σ in the film is therefore the sum of the internal stress σ_0 and of the stress $\Delta\sigma = (\Delta\sigma_{xx}, \Delta\sigma_{yy})$ generated during the experiment. Since $\nu_f < \nu_s < 1$, the increase of external stresses induces an increase of total stress in the (Oy) direction and a decrease in the (Ox) direction of the film. As expected, buckling structures are induced at the sample surface with the increase of external stresses. At the maximum transversal stresses, the structures are mainly composed of straight-sided wrinkles lying perpendicular to the compression axis, as observed in Fig. 4 (white areas). With the release of the external stresses, the buckling structures evolve from straight-sided (a) to either a periodic distribution of bubbles or telephone cords (b). It is here worth noting that many increasing and decreasing stress cycles have been carried out and lead to the same buckling structures. The morphological transitions experimentally observed are thus reproducible and reversible phenomena.

In [24], the selection between bubbles and telephone cord blisters was explained by a critical value of Poissons's coefficient. It is consistent with the stability diagram, since a decrease of the Poisson coefficient is directly related to an increase of the (β_t, β_l) parameters. Nevertheless, this cannot explain the coexistence of the two patterns within the same sample. Moreover, the initially straight-sided wrinkles are not exactly parallel, they differ from one another by a few degrees only. A $\sin^2\psi$ XRD analysis has been carried out on the nickel film. The results confirm that the morpho-

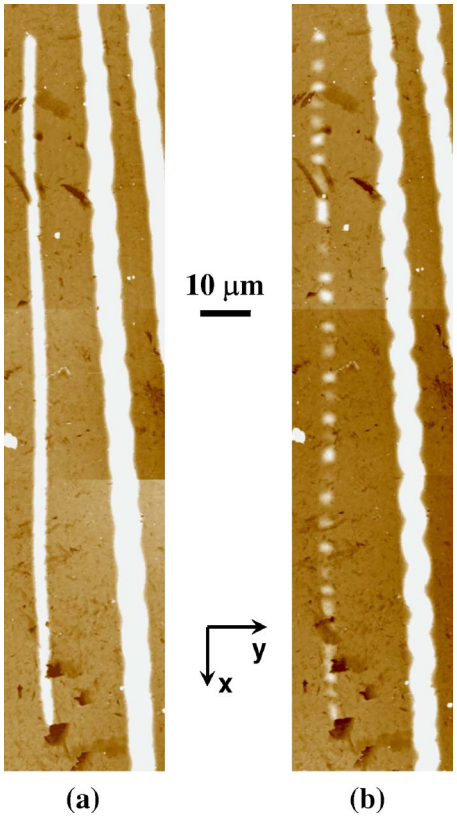

FIG. 4. (Color online) Atomic force microscopy evolution of a nickel 50-nm-thick film under stress. The initial state (a) is associated with higher transversal (Oy) and lower longitudinal (Ox) stresses, compared to the final state (b). The white areas correspond to the buckling structures induced at the sample surface during the compression experiment. Two morphological transitions are observed from straight-sided to either periodic distributions of bubbles (left side) or telephone cord buckling structures (right side).

logical transitions are not ascribed to stress anisotropy in the specimen.

It is here worth noting that any comparison between the FEM diagram and the experimental results has to be carried out in the following frame: in the FEM analysis, the substrate is assumed to be rigid and the stability diagram is built based on this assumption. The diagram is expected to give good results for a wide range of film and substrate systems, as long as the substrate is not too soft compared to the film. Otherwise, its elasticity cannot be neglected and especially the boundary conditions along the delaminated edges are modified; the edges cannot be considered as clamped, since some rotations and displacements coupled to the substrate elasticity are occurring. The effects of the substrate elasticity on thin films buckling have been already studied [25–27], but only for straight-sided wrinkles. Although the diagram should remain qualitatively the same, the substrate effect results in a shift of the stability domain boundaries. The experiments were carried out with nickel films on soft polycarbonate substrates. The substrate softness was required to induce significant stress anisotropy in the thin films, associated with high stress levels, of a few GPa. It allows one to observe the transitions between equilibria and to follow the post critical regime. In spite of the soft substrate, some interesting generic trends can be identified from the AFM experiment; careful interpretations of the experimental results can be made in the frame of the stability diagram. One of these is the influence of the strip width on the nature of the buckling equilibrium.

The telephone cord patterns seem to develop on the largest delaminated strips of the sample (about 6 μm wide), whereas the bubbles are appearing on smaller ones (4 μm wide). The experimental loading sequence has been reported on the stability diagram (see Fig. 3) for 4- and 6-μm-wide strips. In both cases, the maximum compression is exerted by the external device at point (a). In this state, σ_t is large enough compared to σ_l, so that the representative point is located in the straight-sided stability area. As the external compression is progressively released, the loading goes from points (a) to point (b). All final states (b) belong to the bisector of the diagram, since they correspond to the internal isotropic stresses in the film. At the loading end point (b), the 4- and 6-μm-wide strips are in the bubble and telephone cord stability areas, respectively. These predictions from the stability diagram are hence in good agreement with the experimental observations.

For the 4-μm-wide strip, the loading path from points (a) to (b) crosses the boundary separating the straight-sided blisters and the bubbles stability areas. State (b) is not located very deeply in the bubble area. Nevertheless, the numerical pattern shape obtained for this loading is characteristic of distinct and well-formed bubbles. This is because the straight-sided wrinkle to bubbles transition is subcritical [20]. A snap-through occurs during this transition, and the straight-sided wrinkle suddenly collapses into bubbles for a small variation of the loading. The snap-through is also experimentally observed, and the bubble shape observed by AFM in loading state (b) is similar to the computed one. The situation is different for the 6-μm-wide strip, on which the telephone cords appear. The initial state is quite close to the boundary separating the straight-sided blister and the telephone cord areas. This remark is consistent with the AFM observations revealing slight undulations of the wrinkles for this loading. This indicates a telephone cord blister in the incipient buckling regime. As the loading progresses from point (a) to point (b), the part of the longitudinal compression increases; a more pronounced shape of the telephone cord buckle appears, which is characteristic of the post-critical regime with contact areas between the film and the substrate. The transition from the straight-sided to the telephone cord pattern appears to be supercritical from both experimental and numerical points of view.

The FEM stability diagram has been realized within the hypothesis of thin films on rigid substrate. The morphological transitions of buckling structures encountered during the experiments are well explained in this frame, even if the polycarbonate substrates are soft compared to the nickel thin films.

VI. CONCLUSION

In this paper, the different buckling equilibria arising on delaminated thin films have been gathered in families of ho-

mologous equilibria. Knowledge of a particular equilibrium in one of those families allows one to obtain all the other equilibria within the same family. A stability diagram for the various buckling patterns developing on rectangular delaminated strips has been established. This diagram is independent from the strip width and the film thickness. The morphological transitions from straight-sided to bubbles and telephone cords evidenced by the FEM simulation have been observed by AFM on a nickel 50-nm-thick films. The shape diagram shows that, for a strong equibiaxial loading, the telephone cord pattern should be the most commonly observed. The straight-sided and bubble patterns can be more probably seen in films submitted to moderate stress levels associated with a strong anisotropy of stresses and/or of elastic properties. It is consequently shown that the analysis of spontaneous buckling structures frequently observed just after thin film and coating elaboration can be of great interest to determine their mechanical properties in the framework of the stability diagram.

[1] J. Hutchinson and Z. Suo, Adv. Appl. Mech. **29**, 63 (1992).
[2] J. Wang and A. Evans, Acta Mater. **47**, 699 (1999).
[3] J. Hutchinson, M. Thouless, and E. Liniger, Acta Metall. Mater. **40**, 292 (1992).
[4] M. Thouless, J. Am. Ceram. Soc. **76**, 2936 (1993).
[5] A. Evans and J. Hutchinson, Int. J. Solids Struct. **20**, 455 (1984).
[6] J. Hutchinson, J. Mech. Phys. Solids **49**, 1847 (2001).
[7] M. Hu, M. Thouless, and A. Evans, Acta Metall. **36**, 1301 (1988).
[8] G. Gilles and B. Rau, Thin Solid Films **120**, 109 (1984).
[9] P. Green, Am. J. Bot. **86**, 1059 (1999).
[10] G. Gioia and M. Ortiz, Adv. Appl. Mech. **33**, 119 (1997).
[11] M.-W. Moon, H. Jensen, J. Hutchinson, K. Oh, and A. Evans, J. Mech. Phys. Solids **50**, 2355 (2002).
[12] J. Colin, F. Cleymand, C. Coupeau, and J. Grilhé, Philos. Mag. A **80**, 2559 (2000).
[13] M.-W. Moon, K.-R. Lee, K. Oh, and J. Hutchinson, Acta Mater. **52**, 3151 (2004).
[14] F. Paumier, R. Gaboriaud, and C. Coupeau, Appl. Phys. Lett. **82**, 1 (2003).
[15] H. Chen and L. N. Virgin, J. Sound Vib. **278**, 233 (2004).
[16] P. Goudeau, M. George, and C. Coupeau, Appl. Phys. Lett. **84**, 894 (2004).
[17] M. George, C. Coupeau, J. Colin, F. Cleymand, and J. Grilhé, Philos. Mag. A **82**, 633 (2002).
[18] B. Audoly, B. Roman, and A. Pocheau, Eur. Phys. J. B **27**, 7 (2002).
[19] G. Parry, C. Coupeau, J. Colin, A. Cimetière, and J. Grilhé, Acta Mater. **52**, 3959 (2004).
[20] G. Parry, J. Colin, C. Coupeau, F. Foucher, A. Cimetière, and J. Grilhé, Appl. Phys. Lett. **86**, 081905 (2005).
[21] C. Coupeau, J.-C. Girard, and J. Grilhé, J. Vac. Sci. Technol. B **16**, 1964 (1998).
[22] C. Coupeau, J.-F. Naud, F. Cleymand, P. Goudeau, and J. Grilhé, Thin Solid Films **353**, 194 (1999).
[23] ABAQUS, version 6.3, 2003, standard software, a registered trademark of ABAQUS, Inc.
[24] B. Audoly, Phys. Rev. Lett. **83**, 4124 (1999).
[25] G. Parry, J. Colin, C. Coupeau, F. Foucher, A. Cimetière, and J. Grilhé, Acta Mater. **53**, 441 (2005).
[26] B. Huang and T. Zhang, J. Micromech. Microeng. **16**, 134 (2006).
[27] H. Yu and J. Hutchinson, Int. J. Fract. **113**, 39 (2002).